Article ID: 1006-8775(2004) 02-0178-12

INTERANNUAL VARIATIONS OF ATMOSPHERIC HEAT SOURCES AND MOISTURE SINKS OVER THE EQUATORIAL PACIFIC AND THEIR RELATIONS TO THE SST ANOMALIES

LAN Guang-dong (蓝光东), WEN Zhi-ping (温之平), HE Hai-yan (贺海晏)

(*Monsoon and Environment Research Center, Department of atmospheric sciences, Zhongshan University, Guangzhou* 510275 *China*)

ABSTRACT: The interannual variations of atmospheric heat sources and moisture sinks over the Equatorial Pacific and their relations with the SST anomalies are studied using ECMWF reanalysis data from 1979 to 1993. It is found by singular value decomposition (SVD) analysis that the region in the tropical Pacific with high positive correlation between the vertically integrated heat source <*Q*1> anomaly and the SST anomaly, and between the vertically integrated moisture sink <*Q*2> anomaly and the SST anomaly, is mainly located in a long and narrow belt to the east of 170 °E between 5 °S and 5 °N. The analysis of the vertical structure of atmospheric heat sources and moisture sinks shows that the interannual variations of *Q*1, *Q*2 and SST in the equatorial central and eastern Pacific are strongly and positively correlated in the whole troposphere except the bottom (962.5 hPa) and the top (85 hPa) layers. However, in the western Pacific, the interannual variations of *Q*1 below 850 hPa is negatively related to the SST. The correlation coefficient at the level 962.5 hPa reaches even –0.59. In other layers the positive correlation between the interannual variations of *Q*1, *Q*2 and the SST are weak in the western Pacific.

Key words: tropical Pacific; sea surface temperature anomaly; atmospheric heat source

CLC number: P732.6 **Document code:** A

1 INTRODUCTION

ENSO is the strongest signal foretelling climate changes on the interannual scale. Taking place in the tropics, it results in serious climatic anomalies in many parts of the globe[1, 2], as shown in lots of observational analysis and numerical simulation study. The relationship between monsoon variation in East Asia and tropical oceans is especially interested and studied by Chinese researchers, who have achieved fruitful, meaningful results[3, 4]. As an important ring in the study of air-sea interactions and ENSO, diagnostic analysis of anomalous changes in the meteorological fields corresponding to SST anomalies also receives much attention. It is the basis to understand the ENSO cycle and its effects on monsoon and global climate changes. Wang[5] has a detailed study on the variation of meridional and zonal atmospheric circulation cells that are corresponding to the ENSO cycle. In their work on the relationship between interannual variations of meridional wind anomalies and SST anomalies in the tropical Pacific Ocean, Zhang et al[6] reported different wind fields in association with SST anomalies in varying regions and on time different scales. Zhang et al[7]. made an analysis of near-the-surface wind, air temperature and humidity and the correlation between sea surface sensible / latent heat and SST, using NCEP / NCAR data covering the period from 1958 to 1997. It should be noted that research is relatively little on atmospheric heat sources and moisture sinks relating to the ENSO cycle while the

Received date: 2003-04-28; **revised date:** 2004-08-26
Foundation item: National Natural Science Foundation of China (40275026); Part One of National Key Fundamental Research and Development Planning Project (G1998040900)
Biography: LAN Guang-dong (1976 –), male, native from Shaoguan City of Guangdong Province, Ph.D., mainly studying tropical meteorology.

understanding of changes in atmospheric heat sources holds very important significance if one wants to know more about monsoon circulation and global atmospheric circulation during the ENSO episodes. Such instance is found in Li and Yanai (1996)[8]. With the 1985 – 1992 ECMWF TOGA analysis data, they are able to find that heating tends to enhance over the Arabian Sea, Bay of Bengal and western Pacific but to weaken over the equatorial Indian Ocean and equatorial central and eastern Pacific in the years with strong monsoon as defined by Webster and Yang (1992)[8] in their Asian Summer Monsoon Index; heating decreases significantly over South Asia but increases substantially from the equatorial central Pacific and South America coast in the years defined to be with weak summer monsoon in Asia.

With the first version of NCEP reanalysis data (1980 – 1994), Yanai et al[10]. investigated how the atmospheric heat sources and sinks vary on the seasonal and interannual scales between 50°S and 50°N across the globe, with the finding that there is a high and positive correlation between the interannual variations of the vertically integrated values of atmospheric heat sources $\langle Q1 \rangle$ and sea surface temperature (SST), the coefficient being 0.92 and 0.90, respectively, while it is very low in the region of equatorial western Pacific with the coefficient being only 0.44. On the relationship between SST anomalies and atmospheric heat sources, Yanai only takes into account the equatorial region (5°S — 5°N). How are the atmospheric heat sources coupled with the SST in the whole region of tropical Pacific Ocean between 30°S and 30°N? How does the former interact with SST anomalies at different altitudes of the region? In view of the fact that the reanalysis data of ECMWF is better than that of NCEP in some of seasonally averaged climatological features[11] and that Newman et al[12]. also report that the former data are closer to observed precipitation and OLR fields in the Warm Pool region of tropical western Pacific and thus enable better estimates of atmospheric heating fields, the current work uses them to calculate atmospheric heat sources and moisture sinks and studies more of their interannual variations and relationship with the SST to probe into the atmospheric heat sources with ENSO cycles.

2 DATA AND TREATMENT

Data used to determined atmospheric moisture and heat budget are from the reanalysis data of ECMWF (to be shortened as ERA). Being a global gridpoints dataset, it has 17 vertical layers with a horizontal resolution of 2.5° long. × 2.5° lat., and covers four levels of time and a total length of 15 years (1979 – 1993). For the ERA system, a special version of the ECMWF operational data assimilation system is used, which includes a T_{106} spectral forecast model that is divided into 31 layers in the vertical and takes a 3-D semi-Lagrange advection format (Gibson et al., 1999)[13]. ERA data of temperature, humidity and wind field at various mandatory levels at 00:00 and 12:00 GMT are used to derive the apparent heat source $Q1$ and moisture sink $Q2$ as defined by Yanai et al[14]. for 13 layers twice daily and their vertically integrated values over the whole column $\langle Q1 \rangle$ and $\langle Q2 \rangle$. The thirteen layers are at 962.5 hPa, 887.5 hPa, 812.5 hPa, 737.5 hPa, 650 hPa, 550 hPa, 450 hPa, 350 hPa, 275 hPa, 225 hPa , 175 hPa, 125 hPa, and 85 hPa, respectively.

The SST data in the work are taken from reconstructed Reynolds series at a climate analysis center at NOAA-CIRES. Specifically, they are SSTs on monthly mean global gridpoints in each of the months in 1979 – 1993. The dataset has a resolution of 2° long. × 2° lat.

To make the current work comparable with that of Yanai et al[10]., eleven low-pass filter techniques[15] are equally applied in the 15-year month-by-month anomaly series obtained for atmospheric heat sources, moisture sinks and SST in order to highlight the interannual variations.

As the Pacific Ocean is a key area of our concern in the study, the SST data in the region of

125°E – 91°W, 29°S – 31°N are used and that for the atmospheric heat sources and moisture sinks cover 125°E – 90°W, 30°S – 30°N.

3 SST ANOMALIES AND ANAMALOUS FIELDS OF <*Q*1> AND <*Q*2>

How do the SST anomalies in the region 125°E – 90°W, 30°S – 30°N couple with the anomalous fields of <*Q*1>, the vertically integrated value of the atmospheric heat source, and <*Q*2>, the vertically integrated value of moisture? The Singular Value Decomposition (SVD) method is used here. It shows some degree of advantages in extracting two or more dominant coupled signals and has universal adaptability so that it has been widely used in meteorological analysis. The principle of SVD is not elaborated here and the reader can refer to [16] for detail.

The low-pass filtered anomaly field <*Q*1> or <*Q*2> for the Pacific region is taken as the left field A. In view of the fact that if small sample data fields of large number spatial gridpoints were used, the SVD technique would quite possibly yields unreal correlation, the gridpoint intervals are taken to be five latitudes/longitudes in the anomaly fields of <*Q*1> and <*Q*2> to put together a total of *m*1=390 gridpoints in the left field. The low-pass filtered anomalous SST in the Pacific region is taken as the right field B. It is four latitudes/longitudes in gridpoint intervals and has a total of *m*2=549 gridpoints. The total of samples amount to *n*=180 (months) in which *m*2 is about three times of *m*3. The SVD technique is used to determine the distribution patterns of paired diversity correlation between the anomaly of <*Q*1> and <*Q*2> and simultaneous SST anomaly. Tab.1 gives the square covariance contribution by the first four modes and the corresponding time coefficients of the corresponding mode. In the table, (1) indicates that the left field A is the anomaly field <*Q*1> and the right field B is that of SST; (2) indicates that the left field A is the anomaly field <*Q*2> and the right field B is that of SST.

Tab.1 Percentages of square covariance contribution by the first four modes in the SVD analysis scf_k(%) and the time correlation coefficients of corresponding mode $r_k(A, B)$

Modes	scf_k/ %)				$r_k(A, B)$			
	1	2	3	4	1	2	3	4
(1)	89.1	6.2	1.4	1.0	0.92	0.89	0.87	0.91
(2)	88.1	6.1	1.8	1.1	0.90	0.91	0.87	0.90

It is shown in Tab.1 that for (1) and (2), the square covariance contribution by the first mode is both above 88% and correlation coefficients for corresponding modal time are also above 0.90. To verify whether the correlation is significant, the Monte Carlo test[13] is run, i.e. the SVD is built using <*Q*1> and <*Q*2> and random fields. The random fields are composed of computer-generated sequences in normal distribution that have the same number of gridpoints of SST anomaly fields and the same lengths of series. Comparing the quadratic sums of covariance between the anomaly fields of <*Q*1> and <*Q*2> and SST anomaly fields and between the anomaly fields of <*Q*1> and <*Q*2> and random fields with 100 degrees, ($\| C \|^2$), and the percentages for the quadratic sums of interpretive covariance in each of the spatial patterns of SVD pairs, we can infer how the anomaly fields of <*Q*1> and <*Q*2> are correlated with SST anomaly fields and whether the covariance as interpreted by single SVD modes exceeds randomized levels. Following the SVD principle, $\| C \|^2$ stands for the closeness in the overall linkage between any two fields and is related with the characteristic values of the covariance matrixes of the left and right fields in the following way[16]

$$\|c\|^2 = \sum_{i=1}^{R} \sigma_i^2 \qquad (1)$$

Specifically, σ_i is the singular value and R is the number of σ_i that is non-zero. It is known

from the computation that $\| C \|^2$ for the anomaly fields of <Q1> and SST is 1.67E+011 while that for the anomaly fields of <Q1> and the random fields with 100 degrees can be 5.07E+009 at maximum; $\| C \|^2$ for the anomaly fields of <Q2> and SST is 1.49E+011 while that for the anomaly fields of <Q2> and the random fields with 100 degrees can be 4.98E+009 at maximum. It is seen that it is no doubt that on the whole there is linkage between the anomaly fields of <Q1> and <Q2> and SST anomaly fields. It can also be found by comparing the size of the scf_k value that the percentages of the anomaly fields of <Q1> and <Q2> and the quadratic sum of the interpretive covariance in first pair of SVD mode are larger than the corresponding maximum values with the random test, making the linkage reliable. In contrast, other pairs of SVD modes do not pass the significance tests on the 95% significance level. The following part of the text will deal with the diversity correlation distribution patterns of the first mode.

Fig.1a and Fig.1b are the diversity correlation distribution patterns of the first mode for the SVD in the <Q1> anomaly field and simultaneous SST anomaly field. They show that the <Q1> and SST anomaly fields near the equator in the central and eastern Pacific Ocean between 30°S and 30°N are in out-of-phase distribution with other regions (like the northwestern and southwestern Pacific). It is obvious that the distribution pattern of SST in the central and eastern Pacific as shown in Fig.1b is similar to that of the warm episode (El Niño) in the real ENSO cycle[17]. The anomaly distribution of <Q1> as displayed in Fig.1a can be viewed as the anomaly pattern of <Q1> corresponding to the El Niño episode. Superimposing the distribution of the coefficients larger than 0.6 (Fig.1a) and that of the coefficients larger than 0.6, in absolute value, zones of large positive coefficients can be seen overlapping mainly between 5°S and 5°N in areas east of 170°E, and stretches of large negative coefficients can be found overlapping in a small area near 140°E, 12.5°N and some waters close to the Solomon Islands. In these areas, high positive correlation is found between the anomaly fields of <Q1> and SST. Correlation coefficients are 0.70 for the anomalies of <Q1> and SST averaged over the area at 130°E – 140°E, 10°N – 15°N (as indicated by Block A in Fig.1c), 0.86 for those averaged over the area at 170°E – 140°W, 5°S – 5°N in the central Pacific (as indicated by Block B in Fig.1c), and 0.88 for those averaged over the area at 140°E – 90°W, 5°S – 5°N in the eastern Pacific (as indicated by Block C in Fig.1c), respectively. In areas that do not overlap, small correlation coefficients are found between the anomaly fields of <Q1> and SST. The correlation coefficient is only 0.39 for the anomalies of <Q1> and SST averaged over the area at 125°E – 170°E, 5°N – 5°N in the western Pacific (as indicated by Block D in Fig.1c). It can be seen that the results of the current work agree with the conclusion by Yanai et al[10]. Additionally, most of the tropical Pacific where the anomalies of <Q1> and SST are shown, through the SVD analysis, to be in high positive correlation, is within 5°S and 5°N east of 170°E.

Fig.2 depicts the anomaly field of <Q2> and the first mode of the SVD of the anomaly field of SST in the same period. Being generally similar to the anomaly field of <Q1>, it differs only by showing a relatively small overlapped area where the absolute values of the correlation coefficients are above 0.6 in the equatorial eastern Pacific. The coefficients are 0.34, 0.82 and 0.76 respectively for the correlation between the anomaly fields of <Q2> and SST averaged over the western, central and eastern Pacific regions between 5°S and 5°N.

Fig.1d and Fig.2d present the anomalies of <Q1> and <Q2> and the first mode of the SVD of the anomaly field of SST in the same period, with the solid lines for the anomalies of <Q2> or <Q2> and the dashed lines for the anomaly of SST. If the definition of Trenberth (1997) is followed, there were three major El Niño episodes that last relatively long over the 15-year period of interest (1979 - 1993), which appeared in April 1982 – July 1983 (16 months), August 1986 – February 1988 (19 months) and March 1991 – July 1992, respectively; there were two La Niña episodes during the period, occurring in September 1984 – June 1985 (10 months) and May

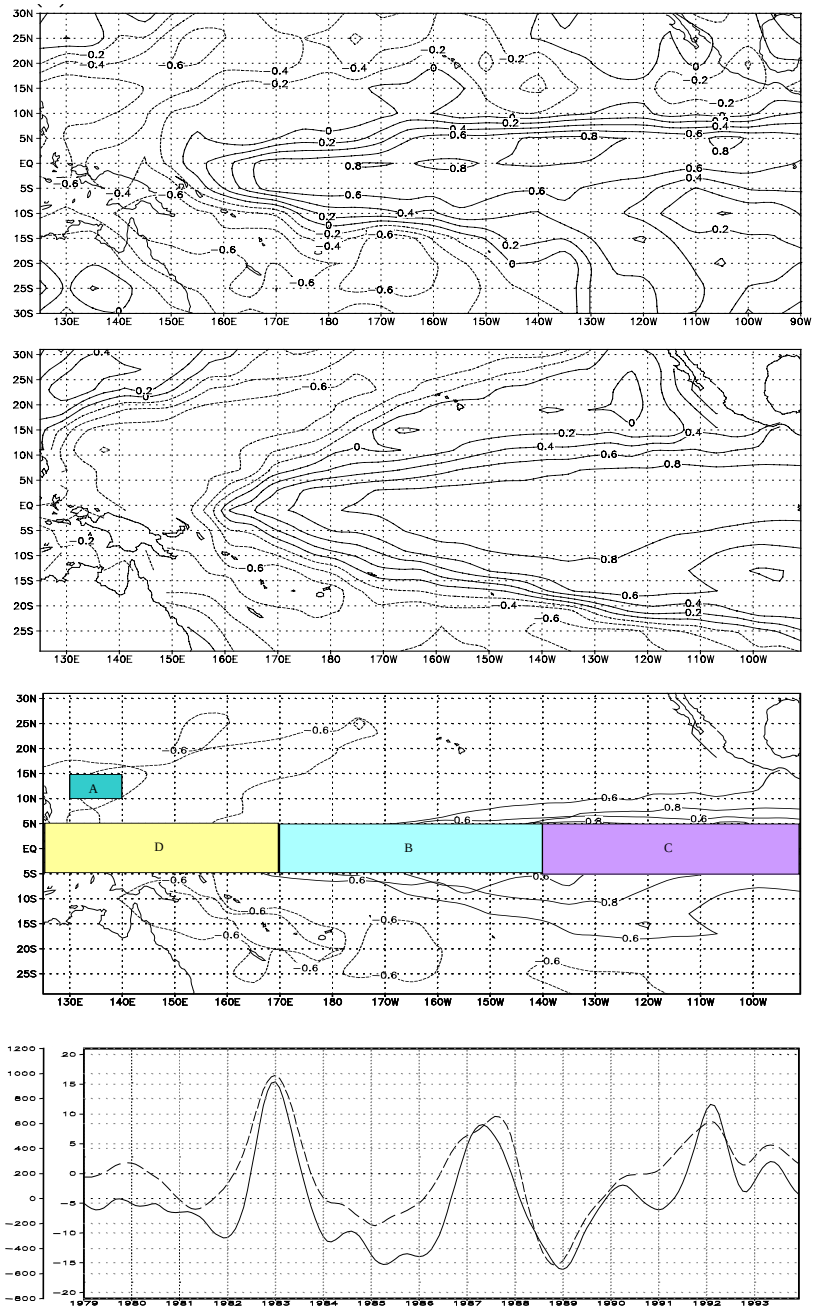

Fig.1 The diversity correlation distribution patterns of the first mode for the SVD in the <*Q*1> anomaly field (a) and simultaneous SST anomaly field (b), which are vertically integrated; (c) is the distribution of the absolute correlation coefficients larger than 0.6 in (a) and (b); (d) is the time coefficients of the first mode, in which the solid line stands for the <*Q*1> anomaly and dashed line for the SST anomaly.

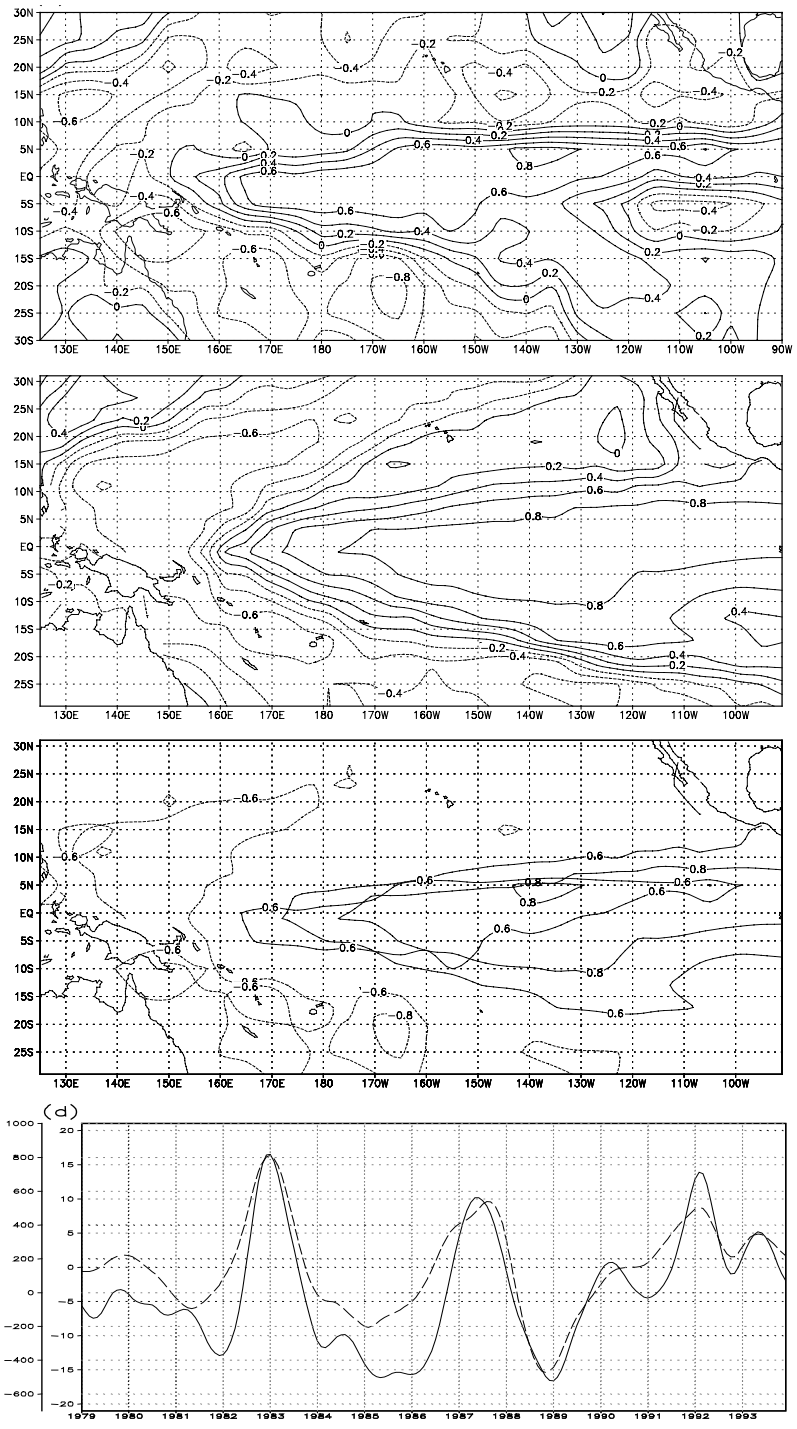

Fig.2 The captions of (a), (b), (c) and (d) are the same as Fig.1 but for the <*Q*1> anomaly field and simultaneous SST anomaly field.

1988 – June 1989 (14 months), respectively. Fig.1d clearly reflects the characteristics of these

episodes. For the 47 years analyzed by Trenberth [18] (1950 – 1996), the ENSO episodes (containing both El Niño and La Niña) take up about 45% of the time, i.e. the tropics is in the warm (El Niño) phase or cold (La Niña) phase most of the time. It can then be known that the first mode of SVD as shown in Fig.1 has substantial background of great importance or is highly representative. Power spectral analysis also shows that periods of 3 to 5 years are the most predominant of all the curves of temporal coefficients.

4 VERTICAL DISTRIBUTION OF ATMOSPHERIC HEAT SOURCE *Q*1 AND MOISTURE SINK *Q*2 AND THEIR RELATIONSHIP WITH SST

Next, let's study the vertical structure of *Q*1, the atmospheric heat source, and *Q*2, the moisture sink, and their relationship with SST. In view of the results above, the areas of interest remain the same as those discussed above, namely, the regions of western, central and eastern Pacific Ocean. Fig.3a, Fig.4a and Fig.5a give the time-altitude cross sections of the low-pass filtered *Q*1 anomalies averaged over these regions; Fig.3b, Fig.4b and Fig.5b give the curves of temporal variation of SST anomalies averaged over individual waters. Tab.2 gives the coefficients of simultaneous correlation in the 180-month time series between mean *Q*1 anomalies and SST anomalies averaged in each layer of the regions.

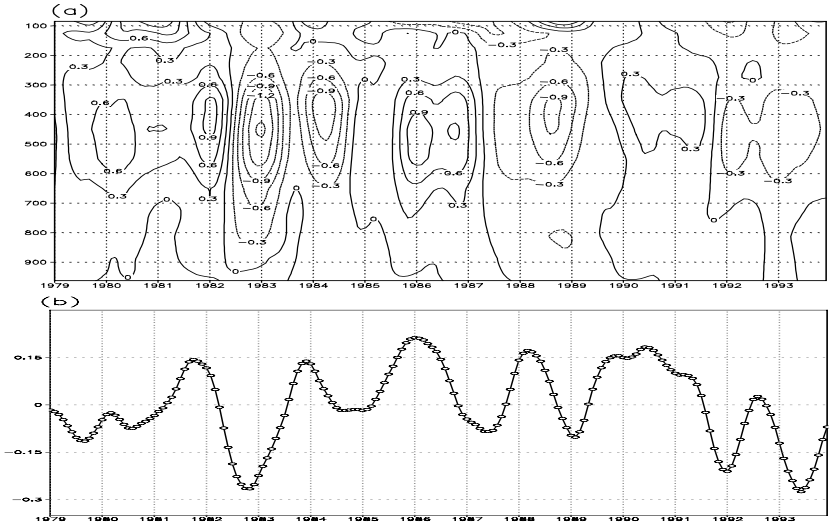

Fig.3 Time-altitude cross section of *Q*1 anomaly averaged over the region of the equatorial western Pacific (125°E – 170°E, 5°S – 5°N) (a) and temporal variation of SST anomalies (b).

From Fig.4 and Fig.5, it is known that the variation of the atmospheric heat source *Q*1 is in good positive correlation with that of SST over the regions of central and eastern Pacific. During the three major El Niño episodes in 1979 – 1993, *Q*1 shows large positive anomalies over nearly the whole column of the troposphere, corresponding to the significant positive anomalies of SST (>0.8°C). The maximum heating appears in the middle and upper levels (600 hPa – 300 hPa). During the two La Niña episodes, however, negative anomalies of *Q*1 occur in the entire troposphere. Except for the bottom level (962.5 hPa) and top level (85 hPa), the correlation coefficients (Tab.2) all stand above 0.70 with the maximum also appearing in the middle and upper levels of the troposphere.

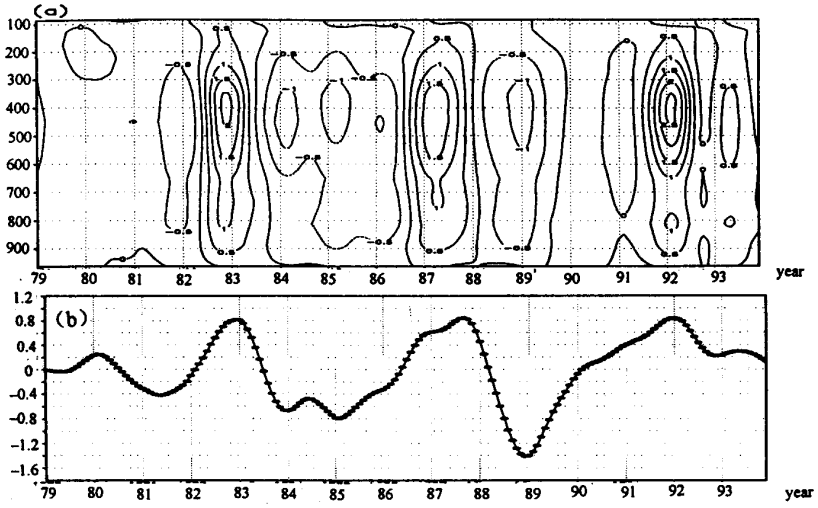

Fig.4 Same as Fig.3 but for the region of equatorial central Pacific (170°E – 140°E, 5°S – 5°N).

Tab.2 Coefficients of the correlation between anomalies of *Q*1 and SST averaged over the region of the equatorial Pacific Ocean

alt. / hPa	962.5	887.5	812.5	737.5	650	550	450	350	275	225	175	125	85
W. Pacific	-0.59	-0.07	0.24	0.47	0.48	0.43	0.44	0.38	0.28	0.30	0.25	0.25	0.06
C. Pacific	-0.10	0.84	0.84	0.83	0.84	0.85	0.86	0.87	0.89	0.88	0.82	0.71	0.06
E. Pacific	0.49	0.85	0.72	0.83	0.85	0.85	0.81	0.85	0.92	0.89	0.87	0.71	0.38

In the western Pacific, things are drastically different (Fig.3). During the three main episodes of El Niño, the atmospheric heat source *Q*1 in the troposphere is either large negative anomaly (1982 – 1987) or weak positive / negative anomaly (1986 – 1987, 1991 – 1992); As shown in the

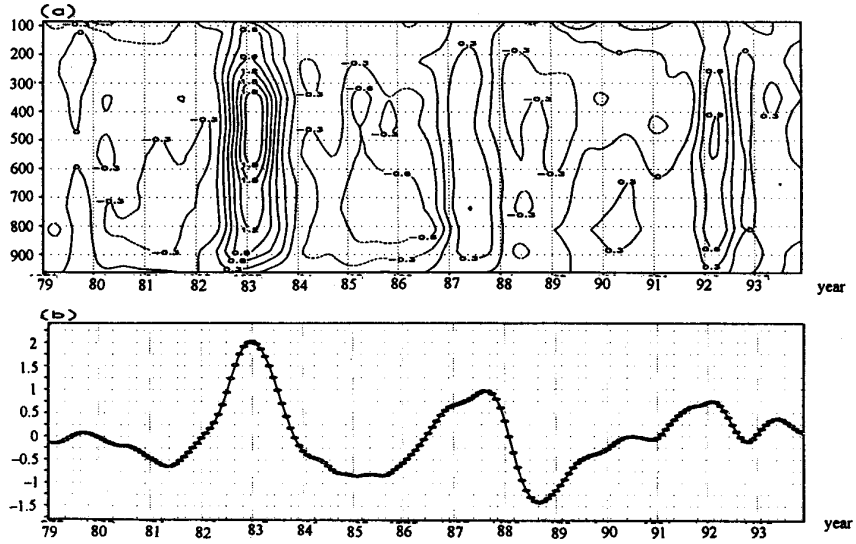

Fig.5 Same as Fig.3 but for the region of equatorial eastern Pacific (140°W – 90°W, 5°S – 5°N).

coefficients of the relationship between $Q1$ and SST, they are in mild positive correlation between 737.5 hPa and 450 hPa (about 0.45); They are even highly negatively correlated at 962.5 hPa (–0.59). What is the same as the central and eastern Pacific is that the maximum heating anomaly centre also appears between 600 hPa and 300 hPa.

Fig.6, Fig.7 and Fig.8 show $Q2$ in different regions of the equatorial Pacific. Tab.3 gives the coefficients of the simultaneous correlation in the 180-month time series between $Q2$ anomaly and SST anomaly averaged over regions of the equatorial Pacific in various levels of the troposphere. It shows that before 1990, the maximum anomaly centers for the central and eastern Pacific appear between 900 hPa and 700 hPa; Two of them appear over the western Pacific, one between 900 hPa and 800 hPa and the other between 600 hPa and 300 hPa; After 1990, the $Q2$ center rises a little to levels between 800 hPa and 600 hPa over the central and eastern Pacific region while a center appears between 700 hPa and 400 hPa over the western Pacific.

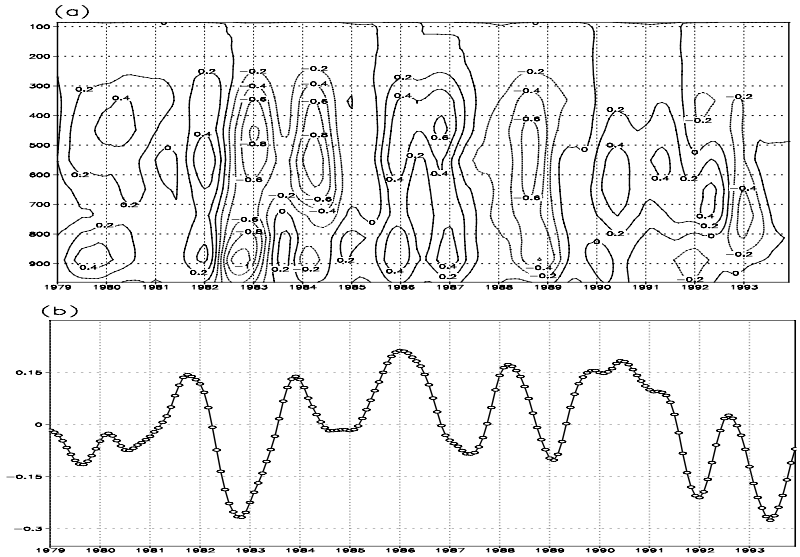

Fig.6 Time-altitude cross section of $Q2$ anomalies (a) and temporal variation curves of SST (b) averaged over the region of western Pacific.

From the coefficients of the correlation between $Q2$ and SST (Tab.3), like the anomaly of $Q1$, the $Q2$ anomaly averaged over the region of central Pacific is highly positively correlated with SST except for the bottom and top levels, all greater than 0.70. In the eastern Pacific, however, it is similar to the case of the central Pacific at all but levels below 800 hPa, in which positive correlation coefficients are relatively small. In the western Pacific, things are similar to the case of $Q1$ in that the positive correlation between $Q2$ and SST is quite weak throughout the whole column of the atmosphere.

Tab.3 Coefficients of correlation between anomalies of $Q2$ and SST averaged over the region of equatorial Pacific

Height / hPa	962.5	887.5	812.5	737.5	650	550	450	350	275	225	175	125	85
W. Pacific	0.40	0.37	0.46	0.35	0.20	0.25	0.25	0.26	0.26	0.20	0.19	0.26	-0.22
C. Pacific	0.53	0.82	0.83	0.79	0.76	0.72	0.74	0.79	0.82	0.84	0.86	0.85	-0.51
E. Pacific	0.22	0.50	0.63	0.83	0.84	0.79	0.67	0.76	0.83	0.85	0.85	0.83	-0.66

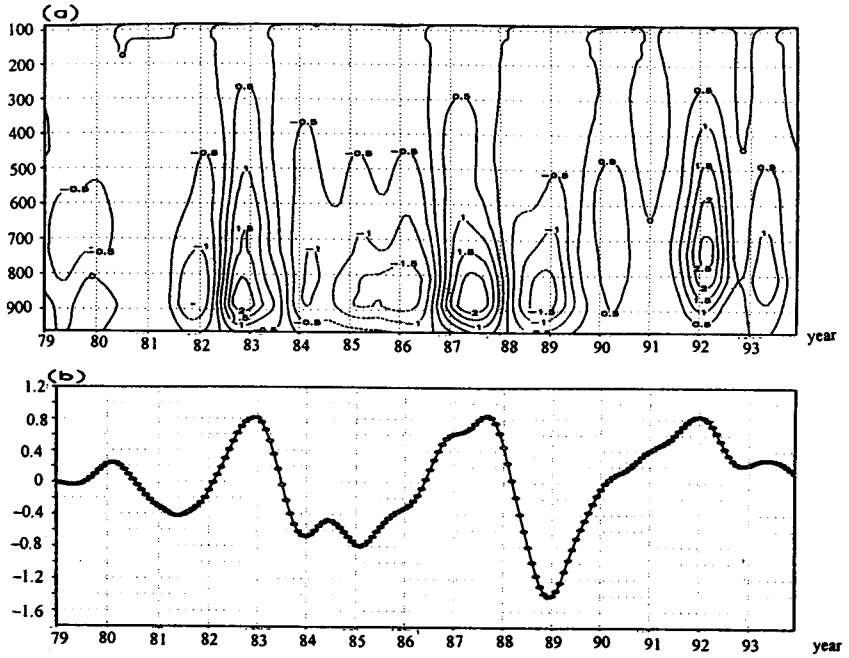

Fig.7 Same as Fig.6 but for the region of equatorial central Pacific.

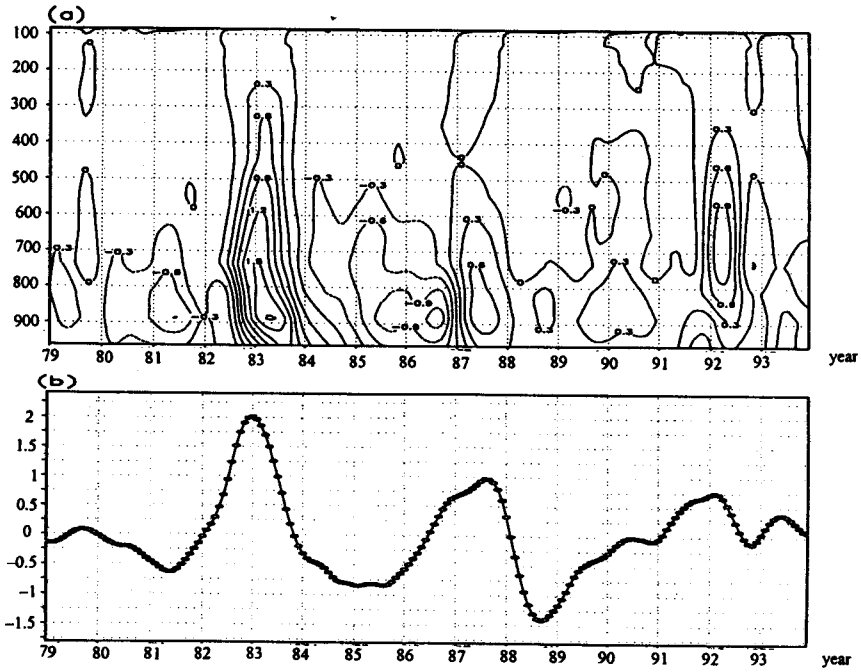

Fig.8 Same as Fig.6 but for the region of equatorial western Pacific.

5 CONCLUSIONS AND DISCUSSIONS

a. With a SVD analysis, we find that for the main coupling modes of the anomaly fields of the vertically integrated atmospheric heat source <$Q1$> and moisture sink <$Q2$> and the SST, their spatial distribution pattern is corresponding to the ENSO cycling distribution pattern. During the El Niño episode, there are significantly positive anomalies of the heat source and moisture sink east of 170°E over the central and eastern Pacific near the equator, which are associated with the anomaly of warm SST; the opposite situation is observed during the La Niña episode.

b. Over the tropical Pacific, the area with high positive correlation between <$Q1$> and <$Q2$> anomaly and SST anomaly mainly concentrates in a strip between 5°S and 5°N east of 170°E.

c. In the central and eastern parts of the equatorial Pacific, the atmospheric heat source $Q1$ shows large positive anomaly nearly throughout the whole troposphere when the SST anomalies are positive during the three El Niño episodes occurred in 1979 – 1993. The correlation coefficients of the two fields are all above 0.70 except for the bottom layer (962.5 hPa) and top layer (85 hPa). The correlation between the moisture sink $Q2$ and the SST anomalies is high and positive except the bottom and the top layers over the central and eastern Pacific. Over the western Pacific, $Q1$ and $Q2$ are in weak positive correlation with the SST anomaly in all layers.

d. From the vertical distribution of $Q1$ and $Q2$ anomalies, we note that maximum heating anomaly centers for the three regions of the equatorial Pacific occur basically in a layer between 600 hPa and 300 hPa. For moisture sinks, however, the maximum anomaly center of $Q2$ appeared between 900 hPa and 700 hPa over the central and eastern Pacific; there appear to have two centers over the western Pacific, one between 900 hPa and 800 hPa and the other between 600 hPa and 300 hPa, in the period prior to 1990. In the period after it, the maximum anomaly center of $Q2$ over the central and eastern Pacific lifted to a layer between 800 hPa and 500 hPa, while there seemed to have one center between 700 hPa and 400 hPa over the western Pacific.

e. An area of high SST, the western Pacific is also a place where deep convection is complicatedly related with SST. Complicated relationships can also be found in atmospheric heating. What kind of favorable condition is there in a strip between 5°S and 5°N east of 170°E in the tropical Pacific that links the heating in the entire atmospheric column of the region with the SST so closely? Fig.9 gives the annual mean distribution of climatological OLR. It shows that the western Pacific is covered with intense convection of deep cumulus while the strip is an area with large OLR values. It shows that deep cumulus convection is absent over the narrow strip in the tropical Pacific. It can be further inferred that cloud clusters over the equatorial Pacific seem to be playing an important role in the linkage between SST anomalies and atmospheric heating anomalies. More study remains on the physical mechanisms responsible for the relationships between atmospheric heating and SST over different parts of the Pacific Ocean.

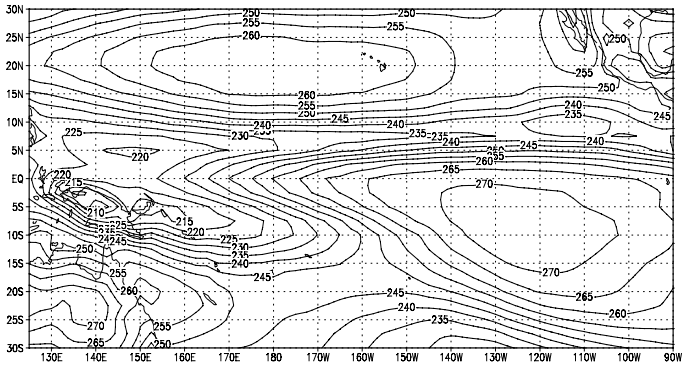

Fig.9 Horizontal distribution of annual mean of climatological OLR in tropical Pacific.

Acknowledgements: Mr. CAO Chao-xiong, who works at the Institute of Tropical and Marine Meteorology, CMA, Guangzhou, has translated the paper into English.

REFERENCES:

[1] WALLACE J M, GUTZLER D S. Teleconnections in the geopotential height field during the northern hemisphere winter[J]. *Monthly Weather Review*, 1981, **109**: 784-812.
[2] SHUKLA J, WALLACE J M. Numerical simulation of the atmospheric response to equatorial Pacific sea surface temperature anomalies [J]. *Journal of Atmospheric Sciences*, 1983, **40**: 1613-1630.
[3] The Earth Science Division of the Committee of the National Natural Science Foundation, Bureau of Resources and Environmental Science of the Chinese Academy of Sciences, Sci/Tech. Education Division of the China Meteorological Administration, Terrestrial Study Department of the Chinese Academy of Sciences .Review and Outlook of the Atmospheric Sciences in the first phase of the 21st century — Proceedings of the Third National Seminar on Pioneering Disciplines of Atmospheric Sciences [C]. Beijing: Meteorological Press, 2000. 101-106, 115-119.
[4] PENG Jia-yi, SUN Zhao-bo. The effects of SST anomalies in eastern Pacific in spring on the evolution of general circulation in spring and summer in East Asia [J]. *Journal of Tropical Meteorology*, 2001, **17**: 398-404.
[5] WANG Chun-zai. Atmospheric circulation cells associated with the El Niño-Southern Oscillation [J]. *Journal of Climate*, 2002, **15**: 399-419.
[6] ZHANG Zu-qiang, DING Yi-hui, ZHAO Zong-ci, et al. Relationships between interannual variation of meridional winds and SST anomalies in the tropical Pacific [J]. *Journal of Tropical Meteorology*, 2002, **18**: 110-120.
[7] ZHANG Wei-qin, QIAN Yong-fu. Key regions of global air-sea interactions and analyses of climatic characteristics within it [J]. 2001, **17**: 23-33.
[8] LI Cheng-feng, YANAI M. The onset and interannual variability of the Asian Summer Monsoon in relation to land-sea thermal contrast [J]. *Journal of Climate*, 1996, **9**: 358-375.
[9] WEBSTER P J, YANG S. Monsoon and ENSO: selectively interactive systems [J]. *Quart J Roy Meteor Soc*, 1992, **118**: 877-926.
[10] YANAI M, TOMITA T. Seasonal and interannual variability of atmospheric heat sources and moisture sinks as determined from NCEP-NCAR Reanalysis[J]. *Journal of Climate*, 1998, **11**: 463-482.
[11] ANNAMALAI H, SLINGO J M. The mean evolution and variability of the Asian Summer Monsoon: comparison of ECMWF and NCEP-NCAR Reanalysis [J]. *Monthly Weather Review*, 1999, **127**: 1157-1186.
[12] NEWMAN M, SARDESHMUKH P D, BERGMAN J W. An assessment of the NCEP, NASA, and ECMWF Reanalysis over the tropical west Pacific warm pool [J]. *Bulletin of the American Meteorological Society*, 2000, **81** (1): 41-48.
[13] GIBSON J K, KALLBERG P, UPPALA S, et al. ECMWF Re-analysis project report series, 1. ERA-15 description, version 2[R], 73.
[14] YANAI M, ESBENSEN S, CHU J -H. Determination of bulk properties of tropical cloud clusters from large-scale heat and moisture budgets[J]. *Journal of Atmospheric Sciences*, 1973, **30**: 611-627.
[15] TRENBERTH K E. Sinal versus noise in the Southern Oscillation[J]. *Mon Wea Rev*, 1984, **112**: 326-332.
[16] WEI Feng-ying. Contemporary Techniques for Statistic and Diagnostic Prediction of Climate [M]. Beijing: Meteorological Press, 1999. 173-184.
[17] CHAO Ji-ping. Dynamics of El Niño and ENSO [M]. Beijing: Meteorological Press, 1993. 187-194.
[18] TRENBERTH K E. The definition of El Nino[J]. *Bulletin of the American Meteorological Society,* 1997, **78**: 2771-2777.
[19] TOMPKINS, LETTERS A M. On the relationship between tropical convection and sea surface temperature[J]. *Journal of Climate*, 2001, **14**: 633-637.